A&A 422, 751–760 (2004)
DOI: 10.1051/0004-6361:20035832

Astronomy & Astrophysics

A new polarimeter for (sub)millimeter bolometer arrays

G. Siringo[1], E. Kreysa[1], L. A. Reichertz[1,2], and K. M. Menten[1]

[1] Max-Planck-Institut für Radioastronomie, Auf dem Hügel 69, 53121 Bonn, Germany
[2] now at University of California, Department of Physics, 366 LeConte Hall, Berkeley, CA 94720, USA

Received 9 December 2003 / Accepted 1 April 2004

Abstract. A new polarimeter concept has been designed to be used together with the bolometer arrays developed at the Max-Planck-Institut für Radioastronomie in Bonn. The new polarimeter has the unique characteristic of being tunable over a wide range of wavelengths and of producing negligible absorption. It has been used at the Heinrich Hertz Telescope to measure the linear polarization of several quasars and of extended sources inside our Galaxy. Some results are presented here. We detected polarization in the quasars 3C 279 and QSO B1633+382. In 3C 279 we also detected polarization variability on a time scale of a week. We also produced maps of three extended sources: the Becklin-Neugebauer/Kleinmann-Low (BNKL) complex in the Orion Molecular Cloud 1 (OMC 1), a filamentary cloud in OMC 3, and the massive star-forming region IRAS 05358+3543. The polarimeter has low spurious polarization and a high modulation efficiency, and the tests at the telescope show that it is well suited to become a permanent facility.

Key words. instrumentation: polarimeters – quasars: individual: 3C 279, 1633+382 – ISM: individual objects: OMC 1, OMC 3, IRAS 05358+3543

1. Introduction

About fifteen years ago the first steps were taken toward submillimeter polarimetry, using single-pixel bolometric receivers. Starting with polarimetry at 100 μm (Werner et al. 1988; Novak et al. 1989) and 1100 μm (Clemens et al. 1990), between then and today the whole submillimeter range has been opened for polarimetry, culminating (for now) with the multiwavelength 300−2200 μm imaging polarimeter of the Submillimetre Common User Bolometer Array (SCUBA; Greaves et al. 2003) on the James Clerk Maxwell telescope.

Linear polarization of submillimeter continuum radiation can be produced by optically thin synchrotron emission in extragalactic objects like radio galaxies and active galactic nuclei or by the partial magnetic alignment of elongated dust grains in interstellar molecular clouds (see Hildebrand 1988). In the latter case, the emission is almost always optically thin. Thus, the bolometer signal is proportional to the dust column density. Practically speaking, this makes dense cloud portions, in particular those associated with star-forming regions and protostellar envelopes, promising targets. In both cases magnetic morphology can be deduced from the directions of the polarization vectors, and polarimetry at millimeter and submillimeter wavelengths can trace the magnetic field in a more direct way than in the optical and radio regimes, where scattering and Faraday rotation can dominate the polarized signal. The goal of submillimeter polarimetry is therefore to map the polarization pattern of these sources with the highest possible angular resolution.

Multi-wavelength polarimetry is particularly desirable as there is a trend for decreasing polarization with increasing optical depth and, thus, decreasing wavelength (e.g. Schleuning et al. 1997). This is probably the result of collisional depolarization in the highest density environments, and thus provides a probe of these.

At submillimeter wavelengths the instabilities of the atmospheric transmission can be large, and ground based polarimetric observations are particularly challenging, as they require high accuracy and, thus, minutes to hours of integration time, because of the weakness of the polarization signal (typically a few percent of the total unpolarized flux). In the last few years great steps forward have been taken in bolometer development and technology, and today we can make use of large arrays of detectors with hundreds of elements.

Here we present a new polarimeter concept, named PolKa after the German *Polarimeter für Bolometer Kameras*, developed by the Bolometer Development Group of the Millimeter and Submillimeter Astronomy Group at the Max-Planck-Institut für Radioastronomie (MPIfR). The work was started with the idea of creating a versatile instrument, capable of giving good results with any of the MPIfR bolometer arrays, at multiple wavelengths, and flexible enough to be installed on

Send offprint requests to: G. Siringo,
e-mail: gsiringo@mpifr-bonn.mpg.de

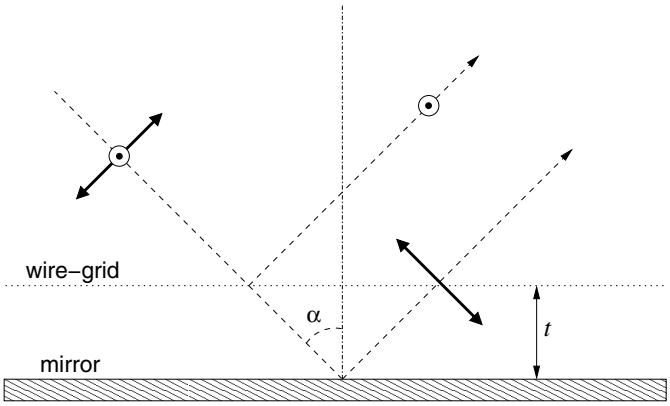

Fig. 1. Scheme of a reflection-type half-wave plate. The incident radiation is divided into two beams with orthogonal polarization states.The two emerging rays will have a relative phase shift proportional to t.

any of the telescopes where MPIfR bolometer arrays are in operation (for details about MPIfR bolometer arrays see Kreysa et al. 2002).

2. Instrument overview and observations

PolKa has many characteristics in common with other polarimeters for millimeter and submillimeter wavelengths. Some of its aspects, however, are unique, such as the unusual solutions of the reflection-type half-wave plate (hereafter RHWP, see Shinnaga et al. 1999) or the continuous spinning technique. In order to extract the polarized signal from the unpolarized foreground it is common to use the modulation/demodulation technique. By means of a polarization modulator, usually a half-wave plate, the polarized component of the incoming radiation is modulated at a precise frequency. If the modulation acts only on the Q and U Stokes parameters of the radiation, the intensity of the latter will be unchanged, at least in the ideal case. Since bolometers are incoherent detectors, they are not sensitive to the phase of the wave but only to its intensity. We need to insert a linear polarizer along the optical path to translate the modulation of the Stokes parameters into a modulation of the total intensity of the transmitted wave. For more details see Siringo (2003).

2.1. The reflection-type half-wave plate

The RHWP consists of two main parts: a wire-grid polarizer and a mirror. By tuning the distance t between the two parts (see Fig. 1), it is possible to produce a phase shift between the two components of polarization, because one is reflected by the wires and the other one by the mirror, causing a difference in path length. The phase shift is given by the simple relation

$$\varphi(\lambda) = 2\pi \frac{t}{\lambda \cos\alpha} \tag{1}$$

where t is the distance between the polarizer and the mirror, α is the angle of incidence of the incoming radiation and λ is the operating wavelength. To have an HWP we assign $\varphi = \pi$ and the value of t for a central operating wavelength λ_0 is given by

$$t = \frac{1}{2}\lambda_0 \cos\alpha. \tag{2}$$

The RHWP works with reflections and we want it to rotate fast: even a small oscillation of the rotation axis can produce a large oscillation of the beam, increasing the noise of the measurements. On the other hand, the RHWP has the advantage that radiation does not pass through it and it can therefore be supported from the back. For these reasons we decided to mount it on a motorized air bearing (model IT103M by INTOP division of Kollmorgen Corp.). This device has an embedded on-axis electric motor and, according to the manufacturer, it is able to maintain the rotation plane within less than 1 μm (Langenbeck 1980). To minimize the errors in positioning the wire-grid parallel to the mirror, we reduced the number of surfaces to be machined with high accuracy to only two: the mirror plate and the upper side of the polarizer frame. The mirror plate is mounted on the air bearing and the distance of the wire-grid can be tuned to the operating wavelength (see Eq. (2)) by means of three Mitutoyo 148-803 micrometer heads: these have a spherical face and a spindle lock, a resolution of 10 μm and an accuracy of 2 μm.

We produced two RHWPs: a small one, about 150 mm in diameter and a larger one, about 250 mm in diameter. The wire-grid polarizers used in the RHWPs were machined in our laboratory. For the smaller one, we produced two identical wire-grids of 146 mm clear aperture, made of Gold coated Tungsten wires with a diameter of 25 μm at a grid step of 100 μm. For the larger version, we produced two identical wire-grids of 246 mm of clear aperture, 20 μm Tungsten wires and 63 μm grid step. The measured mean error in the wire spacing is 18 μm rms.

2.2. The analyzing system

We used two analyzers, mounted in a frame in front of the cryostat window, for easy switching between three different operating modes:

1. horizontal analyzer;
2. vertical analyzer;
3. no analyzer (empty slot) to be used for normal total power measurements.

The analyzers are two identical 65 mm wire-grid polarizers, with wires of 20 μm and a spacing of 50 μm. Before starting an observation, we selected the appropriate analyzer, or none for total power, by sliding the frame in front of the cryostat window.

2.3. Continuous spinning technique and Stokes parameters

Placing a rotating HWP in the beam path will produce a modulation of the Stokes parameters, but the total intensity will remain unchanged. To quantify this assertion, let us consider

the Müller matrix for an HWP rotating at angular velocity ω (Collett 1993)

$$\mathbf{H}(\omega t) = \begin{pmatrix} 1 & 0 & 0 & 0 \\ 0 & \cos 4\omega t & \sin 4\omega t & 0 \\ 0 & \sin 4\omega t & -\cos 4\omega t & 0 \\ 0 & 0 & 0 & -1 \end{pmatrix}. \quad (3)$$

If we compare this matrix with the rotation matrix

$$\mathbf{R}(\vartheta) = \begin{pmatrix} 1 & 0 & 0 & 0 \\ 0 & \cos 2\vartheta & \sin 2\vartheta & 0 \\ 0 & -\sin 2\vartheta & \cos 2\vartheta & 0 \\ 0 & 0 & 0 & 1 \end{pmatrix} \quad (4)$$

we see that it produces a rotation of the polarization vector in the opposite direction and, more importantly, we see that the rotation frequency is doubled: this is the biggest benefit that we gain by using an HWP instead of a linear polarizer. Most of the spurious effects, in fact, will have a frequency equal to the mechanical one, ω, while the polarization signal will be modulated at 4ω resulting in an improved extraction of the signal from foreground and systematic effects. The Stokes vector modulated by the HWP is

$$\mathbf{H}(\omega t)\begin{pmatrix} I \\ Q \\ U \\ V \end{pmatrix} = \begin{pmatrix} I \\ Q\cos 4\omega t + U \sin 4\omega t \\ Q \sin 4\omega t - U \cos 4\omega t \\ -V \end{pmatrix} \quad (5)$$

and we see that the total intensity I of the incoming radiation is not modified because the polarization vector is rotated without any change in its magnitude, at least in the ideal case.

At this point we introduce a fixed linear polarizer into the beam to produce an intensity modulation detectable by the bolometers. The bolometer output is

$$V_{\rm H} = \frac{1}{2}\,(I + Q\cos 4\omega t + U \sin 4\omega t) \quad (6)$$

$$V_{\rm V} = \frac{1}{2}\,(I - Q\cos 4\omega t - U \sin 4\omega t)\,, \quad (7)$$

in the cases of a horizontal and a vertical linear polarizer respectively.

PolKa is used in combination with receivers and amplifiers already existing on the telescope, optimized to work at the frequency of the telescope's chopping secondary mirror (hereafter called wobbler), in most cases 2 Hz. For this reason, the amplifiers have filters cutting off signals below 1 Hz. This will suppress 1/f noise and very slow fluctuations of the offset that is present in the signals. In other words, the bolometer's readout is AC-coupled and the offsets are eliminated. If we apply such a filter to Eqs. (6) and (7) we see that the information about the total intensity I of the signal is lost because it is not modulated. The acquired signals $V_{\rm H}$ and $V_{\rm V}$, in the real case, are given by

$$V_{\rm H} = \frac{1}{2}\,\eta_{\rm H}\,\eta_{\rm HWP}\,g\;(Q\cos 4\omega t + U \sin 4\omega t) \quad (8)$$

$$V_{\rm V} = -\frac{1}{2}\,\eta_{\rm V}\,\eta_{\rm HWP}\,g\;(Q\cos 4\omega t + U \sin 4\omega t)\,, \quad (9)$$

where $\eta_{\rm H}$ and $\eta_{\rm V}$ are the efficiencies of the two linear polarizers, $\eta_{\rm HWP}$ is the efficiency of the HWP and g is the gain factor due to the amplifier. Notice that one will be the opposite of the other when $\eta_{\rm H} = \eta_{\rm V}$.

The choice of the modulation frequency is mainly based on the following two considerations.

- The total power system is optimized for working at 2 Hz because of the mechanical frequency limit of the wobbler. Atmospheric emission fluctuations can have frequencies even higher than 2 Hz, and increasing the modulation frequency would then improve the stability of the signal. In principle, by doing polarimetry without the wobbler we are free to go to much higher frequencies. Nevertheless we should avoid pushing the polarization modulation frequency to values too far beyond 2 Hz, because the bolometer time constant is optimized for that value and the responsivity will drop rapidly with higher frequencies.
- The polarization will be modulated at four times the mechanical frequency: we can easily reach high frequencies without the need of a fast rotation. On the other hand, the error of the position angle of the polarization vector will be four times larger than the mechanical error on the position of the HWP. An accurate determination of the instantaneous position of the HWP is essential.

A typical value of the RHWP mechanical frequency is ω = 4 Hz, corresponding to 16 Hz in polarization modulation. This is higher than typical modulation frequencies produced by a chopping secondary mirror.

2.4. Polarization modulation efficiency (PME)

The efficiency with which the RHWP modulates the Stokes parameters, called polarization modulation efficiency (PME) has been measured in the laboratory. It was determined by comparing the transmission of the system with the transmission measured when a plane mirror was used instead of the RHWP, and using a chopper wheel to modulate the radiation coming from a polarized laboratory source at the same frequency. The laboratory source consists of an absorber (Eccosorb AN72) at liquid Nitrogen temperature chopped by a rotating sector-wheel whose sectors are covered by an absorber at room temperature. In front of the source is a linear polarizer that can be rotated about the optical axis to produce radiation with a well known state of polarization (the error on the angle is about 1°). The measurements were carried out using a bolometric two-channel polarimeter operating at a central wavelength of 1.2 mm. Inside a ^{3}He/^{4}He cryostat, at a temperature of 300 mK, there are two bolometers and a wire-grid polarizer used as a polarization beam-splitter. The optical beam is divided into two orthogonal beams by the cold wire-grid polarizer positioned at 45° to the optical path, such that the horizontal polarization goes straight to one bolometer while the vertical polarization is reflected onto the other one. We found that the RHWP transmits 98% at the maxima and 1.5% at the minima, values mostly due to the distribution of the phase shift among the large bandpass of the receiver ($\Delta\lambda/\lambda \sim 32\%$). The PME is 96.5% when the RHWP is used with MPIfR systems operating at 1.2 mm and will be higher (~98%) for systems with a smaller bandpass like the HHT 19-channel array operating at 870 μm ($\Delta\lambda/\lambda \sim 14\%$). For

comparison, Schleuning et al. (1997) report, for the polarimeter HERTZ, a PME of 75% at 450 μm and 85% at 350 μm and Greaves et al. (2003) report, for the SCUBA polarimeter, a PME of 94% and 97% at 850 μm for the "photometric" and "array" waveplate, respectively.

2.5. Observations and data acquisition

PolKa was tested at the Heinrich Hertz Telescope (hereafter HHT) on Mt. Graham, Arizona, a 10 meter submillimeter telescope equipped with a 19-channel MPIfR bolometer array operating at 870 μm. In May 2001 we made a first test with a small RHWP; a second test with a full size RHWP was made in January 2002. A typical observing session consisted of several steps. First the usual routine scans are performed: a pointing on a strong point-like source, a focus, a second pointing, a skydip. Then, a photometric scan is needed to detect the total flux of the source (Stokes parameter I). This is a standard photometric procedure, chosen according to the source size: on-off for point sources, on-the-fly map for extended sources. In both cases the wobbler modulates the signal at 2 Hz and data are acquired by the HHT's total power backend. Right after the photometric scan, polarization scans are performed to retrieve the other two Stokes parameters Q and U. Before the beginning of the observations the RHWP was accurately tuned to maximize the polarization modulation efficiency. To reduce the systematic effects and for a better removal of the spurious polarization, each polarization scan was made twice, once using the horizontal analyzer and once using the vertical one. Polarization scans were performed following two different observing strategies: on-off, nodding the telescope on and off the source, in the case of point sources; on-the-fly maps in case of extended sources. In both cases we do not wobble the secondary mirror and the polarization of the incoming radiation is only modulated by the spinning RHWP. During polarization scans data are acquired by the polarization backend. At the end of this sequence we performed another skydip and we alternated between total power data acquisition and polarization data acquisition. The polarization backend acquired 23 signals (the bolometer signals plus reference signals used to demodulate the data) at a sampling rate of 512 samples per second resulting in 32 samples per polarization cycle, when the RHWP rotates at 4 Hz. Each data point, once labelled with a timestamp (synchronized by the IRIG-B signal of the telescope's GPS receiver) was stored on a local hard disk in 2-byte-integer format. The time resolution in the data files is ~2 ms. The mechanical angular resolution is given by the sampling rate and by the rotation frequency: when the RHWP rotates at 4 Hz the angular distance between two adjacent samples is 2.°8. An example of the data acquisition is given in Fig. 2: the plot shows the signals detected by the central channel of the array on the blazar 3C 279 during two polarization on-off scans, one performed using the horizontal analyzer and the other performed 16 min later with the vertical analyzer. For each scan, the data points are the mean values of the differences between consecutive pairs of subscans on and off the source, and the error bars represent the standard errors. No further processing has been applied to

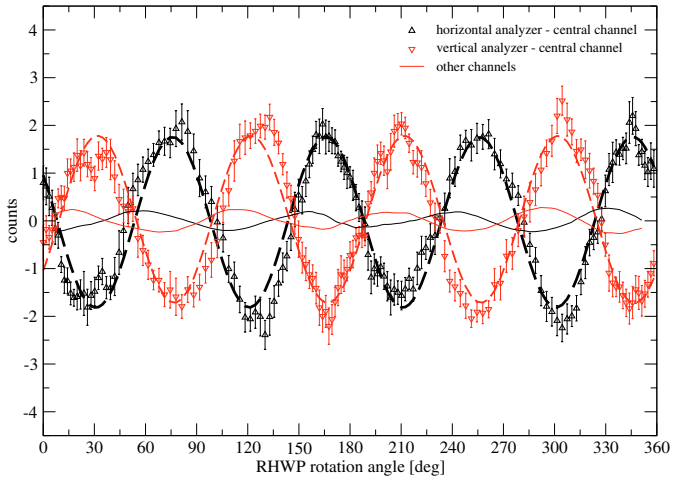

Fig. 2. Example of polarization data acquisition. The source is the blazar 3C 279 observed at the HHT at 870 μm. Upward triangles show data acquired during a polarization on-off scan (2002 January 26, 13:17 UT) performed using the horizontal analyzer, downward triangles are acquired 16 min later with the vertical analyzer. The data refer to the central channel of the array, error bars represent the standard error and the dashed lines are the best sinusoidal fit to the data. The two continuous lines show the mean of the signals detected by the other 18 channels of the array during the two scans.

the data. The RHWP was spinning at 3.5 Hz modulating the Stokes parameters at 14 Hz. We acquired 146 positions per rotation of the RHWP at an angular separation of ~2.°5. For comparison, the polarimeter HERTZ acquires data at 6 fixed position of the HWP at 30° while modulating at 3.1 Hz by using the wobbler (Dowell et al. 1998) and the SCUBA polarimeter acquires data at 16 fixed positions at 22.°5 while wobbling at 7.8 Hz (Greaves et al. 2003).

Each scan in Fig. 2 is made up of 32 subscans, 16 on and 16 off the source. One subscan lasts 21 s and consists of 75 full rotations of the RHWP and comprises 10 950 samples. One complete scan, including the time lost during nodding, lasts about 15 min, the integration time on the source being 336 s, it comprises about 400 000 samples and requires about 20 Mb of computer hard disk storage space in 2-byte-integer format. The plot also shows a sinusoidal fit of the detected signals (dashed lines). The two curves are almost phase-shifted by π relative to each other, as predicted by Eqs. (8) and (9), the phase difference between the two being 175.°8. The deviation of ~4° (from 180°) is due to the apparent rotation of the sky during the 16 min between the two scans caused by the HHT's altazimuthal mount.

2.6. Data reduction and calibrations

New software was written by the authors to reduce the data acquired in the polarization observing modes (see the beam plot in Fig. 3). The data acquired by the PolKa backend contain the information about the Q and U Stokes parameters of the source modulated by the polarimeter. This information has to be recovered by demodulation of the data. This is the same process that the photometric backend performs: the wobbler produces

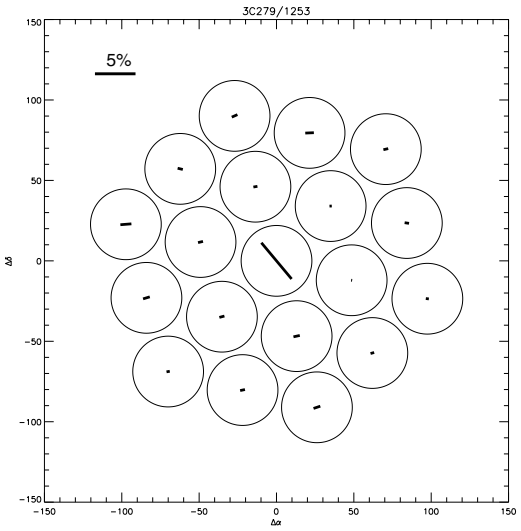

Fig. 3. Example of polarization on-off data reduction: the configuration of the array on the sky is shown together with the measured polarization vectors of each channel. The central channel shows the detection of polarization in 3C 279 (2002 January 26, 13:17 UT).

a modulated signal, the backend acquires the signal and simultaneously averages the differences at the same frequency. This is a demodulation process and its output is proportional to the flux of the source. This is, in general, the principle of "synchronous demodulation", a powerful technique for detecting weak signals affected by strong noise. It is very common to use *lock-in amplifiers* for this type of measurements in the laboratory (Meade 1983). These special amplifiers can recover weak signals hidden in the noise if the signal is modulated at a precise frequency and if an accurate reference signal corresponding to the modulation is supplied. In our special case we take advantage of the fast acquisition made by the PolKa backend to demodulate the data via software using an algorithm called *software lock-in*.

Assume that we perform a polarization scan using the horizontal analyzer:

– The RHWP rotates at frequency ω (e.g. 3.5 Hz) and the modulated signal is given by Eq. (8). After gain and efficiency corrections, it can be written as

$$V(\theta) = \frac{1}{2}(Q\cos 4\theta + U\sin 4\theta) \quad (10)$$

$$\theta = \omega t + \theta_0 \quad (11)$$

where θ is the position angle of the RHWP. For simplicity, in the following calculations we assume $\theta_0 = 0$. In reality, the value of θ_0 must be derived by calibrations of the position angle.

– The polarization backend acquires the data at a sampling rate of S sample/second. In one turn of the RHWP we acquire a set $\{V_i\}$ consisting of N ($\sim S/\omega$) samples (e.g. S = 512 sample/s, ω = 3.5 Hz, N = 146 sample/turn). We know that one turn of the RHWP produces four cycles in the polarization signal. If we know exactly how many acquisition points correspond to each turn of the RHWP we can restore the relative phase between the modulator and the modulated signal and therefore we can demodulate the signal. In this step the software emulates the lock-in amplifier. A reference TTL signal produced by the rotating RHWP is used to retrieve the number of samples in each turn, and thus to lock the phase of the polarization signal.

– The value of one single sample is

$$V_i = V(t_i) = \frac{1}{2}(Q\cos 4\theta_i + U\sin 4\theta_i) \quad (12)$$

$$\theta_i = \omega t_i. \quad (13)$$

– We define the $2N$ quantities

$$S_i = 4\sin 4\theta_i \quad (14)$$

$$C_i = 4\cos 4\theta_i. \quad (15)$$

– We compute the 2 numbers

$$X = \frac{1}{N}\sum_{i=1}^{N} C_i V_i = \frac{2}{N}\left[Q\sum_{i=1}^{N}\cos^2 4\theta_i + U\sum_{i=1}^{N}\cos 4\theta_i \sin 4\theta_i\right]$$

$$Y = \frac{1}{N}\sum_{i=1}^{N} S_i V_i = \frac{2}{N}\left[Q\sum_{i=1}^{N}\cos 4\theta_i \sin 4\theta_i + U\sum_{i=1}^{N}\sin^2 4\theta_i\right].$$

When $N \gg 1$ we have

$$\frac{1}{N}\sum_{i=1}^{N}\cos^2 4\theta_i = \frac{1}{N}\sum_{i=1}^{N}\sin^2 4\theta_i \simeq \frac{1}{2} \quad (16)$$

$$\frac{1}{N}\sum_{i=1}^{N}\cos 4\theta_i \sin 4\theta_i \simeq 0 \quad (17)$$

and we get the demodulated Stokes parameters

$$X \equiv Q \quad (18)$$

$$Y \equiv U. \quad (19)$$

When we perform a polarization scan using the vertical analyzer, the two numbers have the opposite values:

$$X \equiv -Q \quad (20)$$

$$Y \equiv -U. \quad (21)$$

The two demodulated numbers, however, are not yet the Stokes parameters of the radiation coming from the source. We still have to:

– Remove the instrumental spurious polarization.
– Rotate the polarization vector to compensate for the rotation of the source with elevation due to the Nasmyth optical system.
– Rotate the polarization vector to compensate for the parallactic angle of the source.
– Use the calibrations made with a reference source to remove the offset angle θ_0 of Eq. (11).
– Apply the correction for the sky opacity calculated from tabulated values of the zenith opacity measured with the skydip procedure.

All the polarization scans need to be demodulated using this procedure. The results are always the two measured Stokes parameters of the source. In addition to these two, the polarization intensity, polarization degree and position angle are also calculated. To calculate the polarization degree, the software uses tabulated values of the total flux of the sources that have been previously calculated using the usual photometry reduction software.

– Polarization intensity:

$$P = \sqrt{Q^2 + U^2 - f\left(\sigma_Q^2 + \sigma_U^2\right)^2} \tag{22}$$

where f is a debiasing factor that must be determined empirically ($f \sim 1$) to shift to zero the positive bias added by the uncertainties on Q and U (Mack et al. 1997). Given the definition (22) of P, in fact, even when Q and U are affected by Gaussian errors, P will follow a Rice distribution and will be a biased estimator of the true polarization intensity (Wardle & Kronberg 1974; Simmons & Stewart 1985).
The error in P is given by

$$\sigma_P = \frac{1}{P}\sqrt{Q^2\sigma_Q^2 + U^2\sigma_U^2}. \tag{23}$$

– Polarization degree: given the total intensity I of the source and its error σ_I we have

$$p = 100\,\frac{P}{I} \quad [\%] \tag{24}$$

and its error is

$$\sigma_p = 100\,\sqrt{\left(\frac{\sigma_P}{I}\right)^2 + \left(P\,\frac{\sigma_I}{I^2}\right)^2} \quad [\%]. \tag{25}$$

– Position angle:

$$\chi = \frac{1}{2}\,\arctan\left(\frac{U}{Q}\right) \quad [\mathrm{rad}] \tag{26}$$

$$\sigma_\chi = \frac{1}{2}\,\frac{\sigma_P}{P}. \tag{27}$$

Positive angles are measured East of North.

The spurious polarization was estimated by observing the planets Mars and Saturn at different positions in the sky, assuming their emission to be unpolarized. In all the cases the spurious polarization was below 0.8%. The polarized flux was calibrated by total power flux measurements of planets performed with the polarization backend. The polarization position angle was calibrated using a polarized laboratory source: these calibrations are therefore absolute and independent of sky sources. The accuracy in the calibration of the position angle is 0.°8.

2.7. Limitations and sensitivity

The ability to observe very low polarized fluxes is mainly limited by the combination of the following three effects:

– spurious polarization produced by multiple reflections along the optical path and misalignment of lenses and mirrors (optical spurious polarization);
– sidelobe polarization due to the sidelobes of the telescope's main beam;
– spurious polarization due to imperfect tuning and misalignment of the RWHP (systematic spurious polarization).

The amplitude of these spurious signals has been measured to be always less than 1% of the source total flux and can be efficiently reduced, during the data reduction, by subtracting the optical spurious polarization and by removing the signals correlated among the array. The residuals of these effects put a lower limit $p \sim 0.6\%$, on the minimum observable polarized flux.

PolKa is a polarimeter designed to be used in combination with different MPIfR bolometer arrays, at different telescope sites and at multiple wavelengths. The sensitivity of the instrument, therefore, is strictly related to the sensitivity of the bolometers, to the wavelength and to the efficiency of the coupling with the telescope optics. The sensitivity is also different in the two observing modes, polarization on-off and on-the-fly maps. To estimate the sensitivity at the HHT we refer to the polarization on-off on 3C 279. The total flux of the source, during our second telescope campaign, was $I = 14.5 \pm 0.7$ Jy and we measured a polarization degree $p = 5.9\% \pm 0.3\%$ that is a polarized flux $P = 879$ mJy. The plot in Fig. 2 shows the spurious signals detected in the outer channels of the array (continuous lines): after the data reduction, their residuals give a $1\sigma \sim 90$ mJy noise level. In one polarization on-off on 3C 279 we have a 9σ detection in 336 s of integration time on the source. At the HHT, in photometric mode the noise equivalent flux density (hereafter NEFD) of the 19-channel array is 600 mJy/$\sqrt{\mathrm{Hz}}$ under stable weather conditions. Given these numbers, the polarization on-off NEFD at the HHT is 1650 mJy/$\sqrt{\mathrm{Hz}}$.

To estimate the integration time needed to get a signal-to-noise ratio R given the NEFD of the receiver in photometric mode, we can use the general formula

$$t = \left(R\frac{\mathrm{NEFD}}{\eta\, pI}\right)^2 \tag{28}$$

where I is the total flux of the source, p is the fractional polarization (pI is the source polarized flux P) and η is an efficiency factor ($\eta \simeq 0.33$ at the HHT) accounting for the loss of half the signal rejected by the analyzer, and for the decreased responsivity of the bolometers at the polarization modulation frequency, higher than the photometric one. For example, we can estimate the polarization NEFD if PolKa is installed on the IRAM 30 meter telescope on Pico Veleta, Spain, where the MPIfR MAMBO arrays are in operation at 1.2 mm wavelength. The MAMBO bolometers have a NEFD $\sim$ 40 mJy/$\sqrt{\mathrm{Hz}}$: a 1 h integration would give a $R = 3\sigma$ detection for a polarized flux $P = 6$ mJy. In this calculation we assumed the same efficiency we had at the HHT but, given the longer wavelength and the faster bolometers, the efficiency of the system could be better. In polarization on-the-fly map observing mode all N bolometers of the array scan the source. In this case the sensitivity would be better than in polarization on-off mode by a factor $\sqrt{N}$.

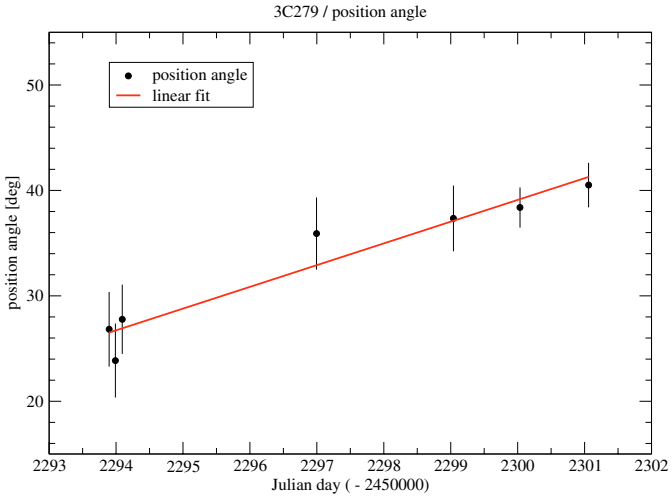

Fig. 4. Polarization position angle of 3C 279 in the 7 days of observations. The variation is ∼14°. The linear fit gives a correlation coefficient of 0.97.

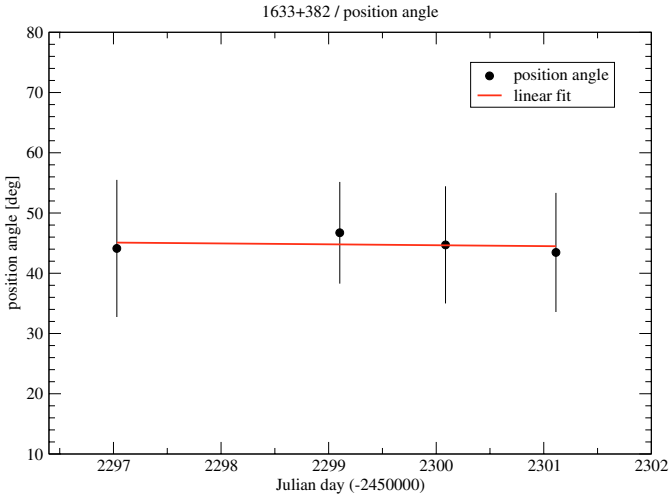

Fig. 5. Position angle of QSO B1633+382 in the 7 days of observations. There is no evidence of variability.

3. Results

3.1. Polarization on-off (point sources)

We detected linear polarization in the two AGNs 3C 279 and QSO B1633+382.

3.1.1. 3C 279

During our second telescope run we measured a total (I) flux density of about 14 Jy, stable within the errors during our week of observations. We also performed 7 polarization scans per analyzer configuration. The mean value of the polarization degree, averaged over the week, is $p = 5.9\% \pm 0.3\%$ after ∼60 min of integration time on the source. However, more interesting than the polarization degree was the behavior of the position angle of 3C 279, for which we detected variability over a time scale of one week. It is well known that the position angle of the polarized radiation emitted by the core of 3C 279 varies with time (see Taylor 1998, 2000; Zavala & Taylor 2001; Homan et al. 2002). The plot in Fig. 4 shows the position angle of 3C 279 during the 7 days of our PolKa observations. The angle shows a variation of about 14°. The plot also shows a linear fit of the data. The correlation coefficient of the fit is 0.97.

3.1.2. QSO B1633+382

The observations QSO B1633+382 of are noisier than those of 3C 279, because the source is weaker and less polarized. The observed polarization degree, after ∼45 min of integration on the source, is $p = 4.6\% \pm 0.5\%$. In this source there is no appreciable variation of the position angle (see Fig. 5). The observed value is $\chi = 44.^{\circ}8 \pm 4.^{\circ}9$, in good agreement with the VLBI measurements at 5 GHz published by Cawthorne et al. (1993).

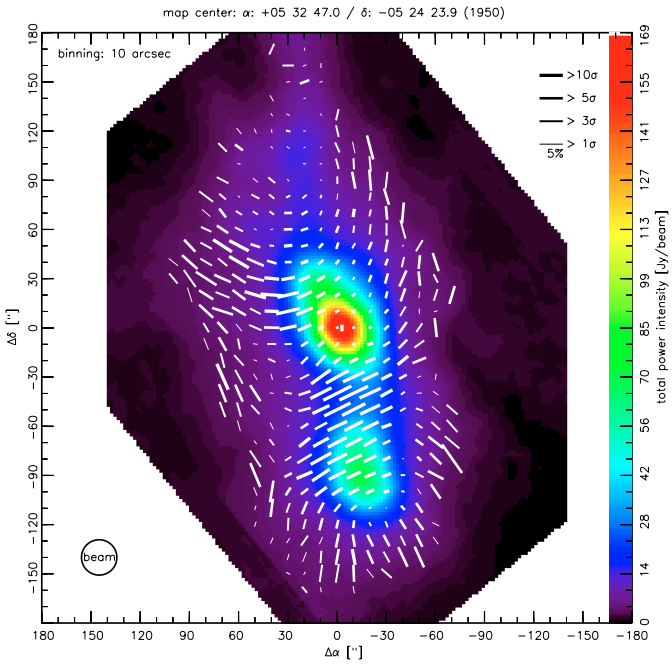

Fig. 6. Polarization degree map of Orion OMC 1 centered on IRc 2. Polarization vectors are rotated by 90° to show the inferred direction of the magnetic field. The length of the vector is proportional to the polarization degree.

3.2. On-the-fly maps (extended sources)

The strong flux and the possibility of comparing our results with previous observations published by other groups made Orion OMC 1 our favorite target. We also made maps of a filament cloud in Orion OMC 3 and of the high-mass star-forming region IRAS 05358+3543.

3.2.1. Orion OMC 1

The map shown in Fig. 6 is the result of 12 scans performed during our 2002 telescope campaign. Each scan covers 360″ × 360″ and required slightly over 30 min, resulting in a total

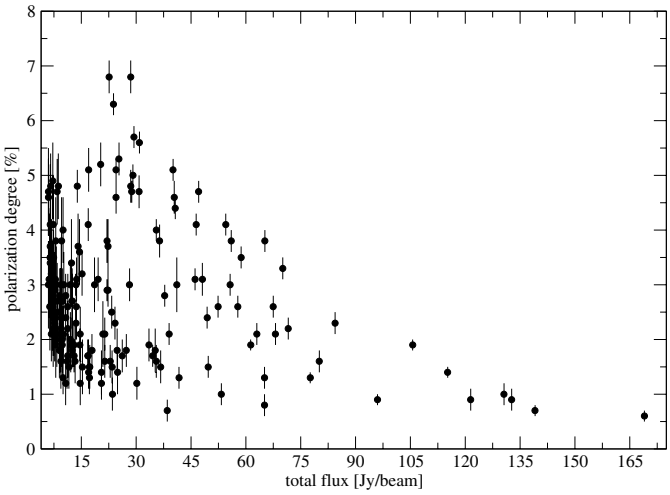

Fig. 7. Depolarization effect observed by PolKa in OMC 1. Detections are better than 3σ.

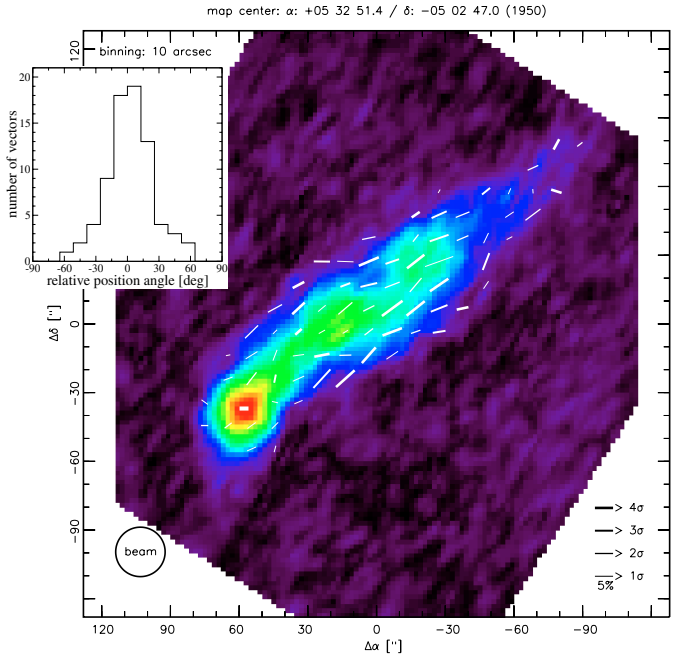

Fig. 8. Polarization degree map of Orion OMC 3. The map is centered between the two clumps MMS3 and MMS4. The brightest clump (bottom left) is MMS6. The histogram shows the distribution of the polarization position angle relative to the position angle of the filament.

integration time of ∼6 h. Figure 6 shows the deduced magnetic field (polarization vectors rotated by 90°). The information shown in the map is manifold. In the background is a total power map of OMC 1. Superposed, polarization vectors are drawn with a resolution of 10″ per vector. The polarization degree is proportional to the length of the vectors. In the top right corner the size of a 5% vector is shown for reference. The position angle is indicated by the direction of the vectors. The quality of the detection is represented by the width of the vectors (see the top right corner for a scale). The map shows only detections that are better than 1σ. The total power threshold in this map is fixed to 4 Jy, 2.4% of the peak. Where the total flux is above this threshold, and no vector is drawn, no meaningful polarization signal was detected. The maximum flux in the map is in the BN/KL area where the total power has a peak of 169 Jy/beam. In the surroundings of the peak 1% of polarization produces a signal of about 1 Jy and a detection at 15σ is possible. We see, however, that the degree of polarization decreases toward areas of the map where the total flux is higher. This is a well known depolarization effect, already observed in other dust clouds (see, for example, Matthews et al. 2001; Houde et al. 2002). Figure 7 shows the depolarization effect observed by PolKa in OMC 1. The magnetic field directions in our OMC 1 map are in excellent agreement with those determined by Coppin et al. (2000) at 850 μm and by Schleuning et al. (1997) at 350 and 450 μm, although our polarization degrees are higher than those at 350 and 450 μm, as expected from the arguments mentioned in the introduction.

3.2.2. Orion OMC 3 MMS3/MMS4

Besides OMC 1, in the Orion A giant molecular cloud there are two other large areas of interest, OMC 2 and OMC 3, that are the consecutive parts of OMC 1 going northwards along the Integral-Shaped Filament (Bally et al. 1987). In the northern part of OMC 3 7 embedded cores have been identified by Chini et al. (1997), named MMS1 to MMS7. Given the results of Matthews et al. (2001) we decided to scan this area, to test the polarimeter on a dust source of known polarization but weaker than OMC 1. Our polarization map, which is shown in Fig. 8, is centered between the two clumps MMS3 and MMS4 (see Fig. 1 in Chini et al. 1997, for reference). Only three scans were performed, and the total integration time is only 1.5 h, resulting in a poor signal-to-noise ratio. The best detections in the map are at $\simeq 4\sigma$, but most of the vectors have signal-to-noise between 1 and 3σ. This map is presented here only to show that even if the integration time was very short, the polarization vectors show good consistency in the detected position angle. The histogram at the top-left corner shows the distribution of the polarization position angles of the vectors relative to the position angle of the filament between the two cores MMS1 and MMS6, ∼130° E of N. Our map shows, indeed, a good agreement with the results published by Matthews et al. (2001) at 850 μm and by Houde et al. (2003) at 350 μm.

3.2.3. IRAS 05358+3543

In recent years massive outflows have been investigated in detail because they can provide information about the innermost parts of star-forming regions. The source IRAS 05358+3543 is an extremely young and deeply embedded high-mass protostellar object. This source is part of a recent statistical work on massive outflows by Beuther et al. (2002b). They found that low-mass correlations of outflow and core parameters continue up to the high-mass regime, suggesting that similar star formation processes are responsible for forming stars of all masses. However, massive star formation sites are on average more distant than well known low-mass sources, and thus their angular sizes are smaller in spite of their larger linear sizes.

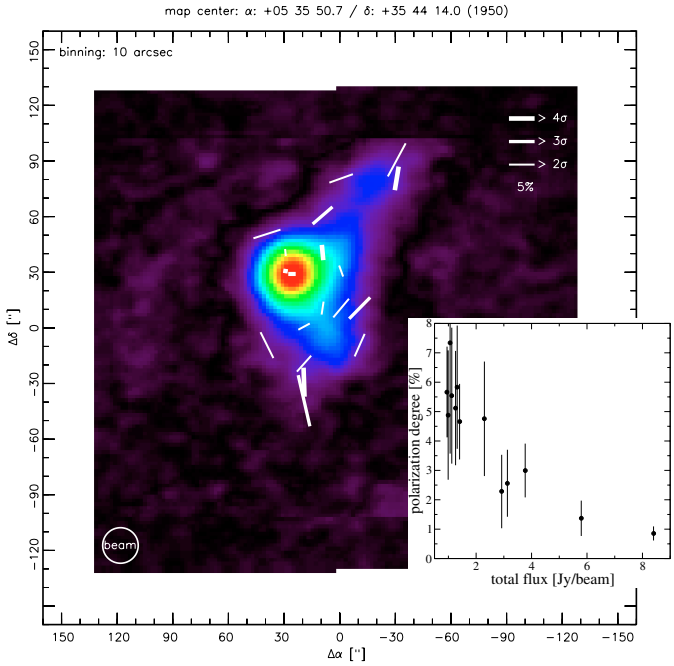

Fig. 9. The first polarization map of IRAS 05358+3543. Polarization vectors are rotated by 90° to show the inferred magnetic field. The plot at the bottom right corner shows the observed depolarization.

This indicates that high angular resolution is needed to disentangle real source and outflow structures. One solution is to study these sources with interferometric techniques at millimeter and submillimeter waves. Polarization maps of the continuum emission, at the same wavelengths, can be a powerful way to obtain information about the order of the structures in the source, and could be a valid complement to interferometric observations. Figure 9 shows the first detection of polarization in the source IRAS 05358+3543. We performed 8 scans on this source, collecting 4 h of integration time. The size of the map is 320″×320″. At the HHT the 345 GHz flux peak of the source was 8.4 ± 1.2 Jy/beam, at $\Delta\alpha = 28''$, $\Delta\delta = 33''$ from the absolute IRAS positions given by Sridharan et al. (2002), where our map is centered. The map shows the polarization vectors rotated by 90° to show the deduced magnetic field directions. All polarimetric detections in the map are better than 2σ. The polarization signal is subject to the depolarization effect going toward the most intense areas of the source, behaving in the same way as it was found to behave in low-mass star-forming regions. On the north and south edges of the cloud, however, we can see that the strongest polarization signals are aligned along the direction deduced by Beuther et al. (2002a) for the larger molecular outflows of the source (see Fig. 4 in Beuther et al. 2002a). This is an interesting result that is worthy of further investigation with our polarimeter, at different angular scales and at different wavelengths.

4. Conclusions

Our polarimeter uses only metallic reflections and this gives it very low insertion losses and a high efficiency. PolKa is tunable: by simply adjusting three screws one can switch from one operating wavelength to another. In addition, PolKa's tunability can be used to transform the half-wave plate to a quarter-wave plate with ease and the same instrument can also be used to perform circular polarization observations. The radiation is modulated directly by PolKa, without the need for a chopping secondary mirror. The modulation frequency can be much higher than when using a wobbler, and the polarimeter can be used even at telescopes with a fixed secondary mirror. Furthermore, the polarization signals are restored by digital phase-sensitive detection and not by fitting a sine wave to a noise-dominated signal, as commonly done in other polarization experiments. The tests at the telescope showed that PolKa is able to produce high quality polarization data. In particular, it can produce large polarization maps with high signal-to-noise in a relatively short time. PolKa as it is will be installed on the IRAM 30 meter MRT, where the MAMBO (Max-Planck-Millimeter-Bolometer array) receiver is operating at 1.2 mm. An improved version of PolKa will be installed on the new submillimeter telescope APEX in the Atacama desert in Chile in combination with the new array LABOCA (Large Bolometer Camera), made of 300 bolometers operating at 870 μm.

Acknowledgements. The authors would like to thank: Manfred Tonutti (Rheinisch-Westfälische Technische Hochschule, RWTH, Aachen, Germany), who suggested the way to upgrade our wire-grid machine to larger grid sizes; the *Friends of the Telescope* and the *Astronomers on Duty* at the Heinrich Hertz Telescope, for their support during our observations; Giuseppe Cimò (formerly MPIfR, now at University of Tasmania, Hobart, Australia) for his participation to the 2002 telescope campaign. We also thank the referee Jane Greaves for detailed reading of the manuscript and useful suggestions, and the language editor Jet Katgert.

References

Bally, J., Stark, A. A., Wilson, R. W., & Langer, W. D. 1987, ApJ, 312, L45
Beuther, H., Schilke, P., Gueth, F., et al. 2002a, A&A, 387, 931
Beuther, H., Schilke, P., Sridharan, T. K., et al. 2002b, A&A, 383, 892
Cawthorne, T. V., Wardle, J. F. C., Roberts, D. H., Gabuzda, D. C., & Brown, L. F. 1993, ApJ, 416, 496
Chini, R., Reipurth, B., Ward-Thompson, D., et al. 1997, ApJ, 474, L135+
Clemens, D. P., Kane, B. D., Leach, R. W., & Barvainis, R. 1990, PASP, 102, 1064
Collett, E. 1993, Polarized light: fundamentals and applications (New York: Marcel Dekker, Inc.)
Coppin, K. E. K., Greaves, J. S., Jenness, T., & Holland, W. S. 2000, A&A, 356, 1031
Dowell, C. D., Hildebrand, R. H., Schleuning, D. A., et al. 1998, ApJ, 504, 588
Greaves, J. S., Holland, W. S., Jenness, T., et al. 2003, MNRAS, 340, 353
Hildebrand, R. H. 1988, QJRAS, 29, 327
Homan, D. C., Ojha, R., Wardle, J. F. C., et al. 2002, ApJ, 568, 99
Houde, M., Bastien, P., Dotson, J. L., et al. 2002, ApJ, 569, 803
Houde, M., Dowell, C. D., Hildebrand, R. H., et al. 2003 [arXiv:astro-ph/0312365]

Kreysa, E., Gemünd, H.-P., Raccanelli, A., Reichertz, L. A., & Siringo, G. 2002, in Experimental Cosmology at Millimetre Wavelengths: 2K1BC Workshop, Breuil-Cervinia, Valle d'Aosta, Italy, 9−13 July, 2001, ed. M. De Petris, & M. Gervasi, AIP Conf. Proc., 616, 262
Langenbeck, P. 1980, Sonderdruck aus Industrie Diamanten Rundschau IDR 2
Mack, K.-H., Klein, U., O'Dea, C. P., & Willis, A. G. 1997, A&AS, 123, 423
Matthews, B. C., Wilson, C. D., & Fiege, J. D. 2001, ApJ, 562, 400
Meade, M. L. 1983, Lock-in amplifiers: principles and applications (P. Peregrinus on behalf of the Institution of Electrical Engineers)
Novak, G., Gonatas, D. P., Hildebrand, R. H., Platt, S. R., & Dragovan, M. 1989, ApJ, 345, 802
Schleuning, D. A., Dowell, C. D., Hildebrand, R. H., Platt, S. R., & Novak, G. 1997, PASP, 109, 307
Shinnaga, H., Tsuboi, M., & Kasuga, T. 1999, PASJ, 51, 175
Simmons, J. F. L., & Stewart, B. G. 1985, A&A, 142, 100
Siringo, G. 2003, Ph.D. Thesis, Rheinische Friedrich-Wilhelms-Universität Bonn
Sridharan, T. K., Beuther, H., Schilke, P., Menten, K. M., & Wyrowski, F. 2002, ApJ, 566, 931
Taylor, G. B. 1998, ApJ, 506, 637
Taylor, G. B. 2000, ApJ, 533, 95
Wardle, J. F. C., & Kronberg, P. P. 1974, ApJ, 194, 249
Werner, M. W., Davidson, J. A., Morris, M., et al. 1988, ApJ, 333, 729
Zavala, R. T., & Taylor, G. B. 2001, ApJ, 550, L147